Metal-to-metal charge-transfer transitions in Prussian blue hexacyanochromate analogues

Metal-to-metal charge-transfer transitions in Prussian blue hexacyanochromate analogues

David M. Rogers and J. Olof Johansson*

Edinburgh and St Andrews Research School of Chemistry (EaStCHEM), University of Edinburgh, David Brewster Road, EH9 3FJ, Edinburgh, UK

**Corresponding author. Email address: olof.johansson@ed.ac.uk*

Abstract

Time-dependent density functional theory (TD-DFT) calculations are presented for a series of Prussian blue analogues (PBAs) based on hexacyanochromate in order to investigate optical metal-to-metal charge-transfer (MMCT) transitions. PBE0 hybrid DFT calculations at fixed geometry were carried out on binuclear units of $(CN)_5$-M_A-NC-Cr^{III}-$(CN)_5$, with M_A = V^{II}, V^{III}, and Cr^{II}. The MMCT transitions occurred at 743 nm for the V^{II}-Cr^{III} PBA and at 780 nm for the V^{III}-Cr^{III} PBA. The ordering of the transition energy and strength for these analogues agreed with data available in the literature. The transition for the Cr^{II}-Cr^{III} MMCT was found to occur at 284 nm. This study shows that TD-DFT is a powerful method to study optical properties of PBAs and that the results for the relatively simple binuclear cluster are comparable to solid PBAs, where MMCT transitions are typically the dominant feature in the visible part of the absorption spectrum.

Keywords: Time-dependent density functional theory; Prussian blue analogues; charge-transfer transitions; multifunctional materials; optical properties

1. Introduction

Switching functional molecular materials to metastable states using external perturbations is of great interest for future electronics and information storage technologies. A promising class of materials for this purpose are Prussian blue and its analogues (PBAs), which are coordination polymers comprising transition metal ions linked by cyanide ligands in a rock-salt structure [1]. The general formula is $C_cA_a[B(CN)_6]_b \cdot nH_2O$ (C=alkali cation, A,B = transition metal ions). The PBAs typically display bright colours due to strong metal-to-metal charge-transfer (MMCT) transitions in the visible spectrum. The charge-transfer (CT) occurs between ions A and B, and can approximately be represented as

$$\mathrm{M_A^n - NC - M_B^m} \overset{h\nu}{\rightarrow} \mathrm{M_A^{(n-1)} - NC - M_B^{(m+1)}},$$

where n and m are the corresponding formal oxidation states. In this example, the A ion is reduced as a result of CT from the B ion. The MMCT transition can be very important in controlling the physical properties of PBAs as a means of external optical stimulus. For example, MMCT can lead to meta-stable states that affect the magnetic properties, producing interesting photomagnetic effects [2,3]. On the other hand, it is also possible to turn off the MMCT transition electrically making use of the electrochromic properties of some PBAs. For example, the bright blue colour of Prussian blue itself (containing Fe^{III}-Fe^{II}) can be completely switched off by applying a small potential[4,5]. It is also possible to combine magnetic and electrochromic properties, as is the case for the V-Cr PBA [6–8]. These examples demonstrate one of the many fascinating aspect of PBAs, namely their multifunctional nature. With the capabilities of modern quantum chemistry[9–11], it is becoming possible to quickly screen the properties that control MMCT transitions in complex materials and molecules. Here, we present results of a TD-DFT computational study of the MMCT of a series of PBAs.

Robin and Day have classified mixed-valence compounds into three types, where PBAs typically fall into Class II [12]. This means that the valence electrons are not fully localised on

the metal ion sites at elevated temperatures. In fact, the intensity of MMCT transitions can be shown to be proportional to the degree of delocalisation α between the metal ions A and B. The total wavefunction Ψ_0 can be written as a superposition of the fully localised wavefunction Ψ_0' and a wavefunction Ψ_l where the optical electron is fully localised on the other metal ion [12], according to

$$\Psi_0 = \sqrt{1-\alpha^2}\Psi_0' + \alpha\Psi_l.$$

For Prussian blue, the value of α is on the order of 1 %. It can be shown that the transition dipole moment is proportional to the delocalisation factor α [12,13], which in turn depends on the mixing and energy difference between the fully localised state and the transferred-electron-state. This has been thoroughly described by several authors based on symmetry arguments [12–14]. However, with the emerging field of functional materials and the important role of MMCT in their optical properties, it is interesting to revisit the MMCT of PBAs using TD-DFT methods.

There are several PBAs reported in the literature with the corresponding MMCT occurring at different spectral positions in the visible spectrum. For example, in electrochemically deposited thin films of $\left(\mathrm{Fe}_{\mathrm{x}}^{\mathrm{II}}\mathrm{Cr}_{1-\mathrm{x}}^{\mathrm{II}}\right)_{1.5}[\mathrm{Cr}^{\mathrm{III}}(\mathrm{CN}_6)]$ PBAs, where x ranges from 0 to 1, the colour of the films could be tuned by the stoichiometry producing films that were either colourless (x = 0), violet (x = 0.2), red (x = 0.4), or orange (x = 1) [15]. A more attractive system to investigate in a computational study, is the ternary $\mathrm{K}_{\mathrm{a}}^{\mathrm{I}}\mathrm{V}_{\mathrm{x}}^{\mathrm{II/III}}\mathrm{Cr}_{1-\mathrm{x}}^{\mathrm{II}}\,[\mathrm{Cr}^{\mathrm{III}}\mathrm{CN}_6]_{\mathrm{b}}$ PBA [16] due to the relatively small number of electrons of the d^3 ions Cr(III) and V(II), and the d^2 ion V(III). For the case when x = 1, the MMCT occurs either at 660 nm (Cr^{III} - V^{III}) or 540 nm (Cr^{III} - V^{II}) [8,17,18] and provides an interesting case to study the MMCT as a function of vanadium oxidation state. In the case when x = 0, the MMCT has been assigned to occur at 510 and 610 nm [15]. These transitions are not fully understood since the peaks that have been assigned as MMCT in the visible are rather weak and, furthermore, in another study the MMCT was assigned to occur in the UV at around 380 nm [19].

We recently carried out TD-DFT computations to support the assignment of the optical spectrum of the V-Cr PBA [20]. We used a simplified model of the PBA by carrying out quantum chemical calculations on a binuclear unit. In this model, both metal ions are surrounded by cyanide ligands, giving the formula $(CN)_5$-M_A-NC-Cr^{III}-$(CN)_5$ with M_A = V^{II}, V^{III}, and Cr^{II}. This approach worked surprisingly well considering its simplicity. In this paper, we have expanded the range of variable inputs in the calculations and studied the effects of initial geometry and spin state of the open-shell system. We found that the TD-DFT calculations could reproduce the relative energy and oscillator strengths of the MMCT of $V^{II/III}$-Cr^{III} PBA in good agreement with previously published experimental work. The larger oscillator strength for the MMCT of V^{II}-Cr^{III} vs V^{III}-Cr^{III} was explained by the larger degree of delocalisation of the optically active orbitals in the V^{II}-Cr^{III} PBA. We found that the MMCT for Cr^{II}-Cr^{III} occurred in the UV involving the HOMO-2 orbitals, which are more localised than the HOMO (which in turn is responsible for the magnetic properties). Interestingly, in Cr^{II}-Cr^{III} PBAs, the delocalised HOMO gives rise to a relatively high magnetic ordering temperature ($T_c \approx 240$ K[21–25]) whereas the more localised HOMO-2 gives rise to a weak oscillator strength for the MMCT.

2. Method

To study PBAs using “Gaussian-based” quantum chemical techniques we chose a single binuclear unit with, initially, a fixed geometry, comprising one V with five CN^- ligands (with N pointing toward V), one Cr with five CN^- ligands (with C pointing toward Cr) and one bridging CN^- ligand (with N toward V and C toward V). This model has been adapted previously in DFT studies of the magnetic properties of a number of different PBAs[22–25]. This monomeric unit possesses C_{4v} symmetry. The charge of the cluster is given by the sum of the oxidation states of the metal ions and the 11 negatively-charged cyanide ligands. The bond lengths chosen for the model monomeric unit are those as determined by Garde *et al*.

using x-ray absorption data [17]. The same bond length was also used for the Cr^{II}-Cr^{III} calculations. The bonds N-C, C-Cr and N-V have lengths of 1.15, 2.06 and 2.12 Å, respectively. This corresponds to a V-Cr distance of 5.33 Å. For the V part of the monomeric unit, the C ends of the cyano ligands were uncapped. Figure 1 depicts the binuclear unit of V-Cr PBA used to perform the calculations. In addition, a 'stretched' geometry where the V-Cr distance is 5.75 Å was considered by having the bridging bond lengths for V-N, N-C and C-Cr of 2.33, 1.15 and 2.27 Å, respectively. In the calculations for Cr^{II}-Cr^{III} PBA, we chose Cr^{II} in the N site and Cr^{III} in the carbon site. Experimentally, the oxidation states of the Cr-Cr PBA can be quite difficult to determine[19,26] and so whenever we refer to experimental data published in the literature we do not give the oxidation state.

Gaussian 09 [18] was employed to perform TD-DFT calculations using the PBE0 hybrid exchange-correlation functional [19] with the 6-311G(d) basis set [20] for V and Cr ions, and the 6-31G(d) basis set [21,22] for C and N atoms. The unrestricted formalism was used for open shells and for closed-shell V^{II}-Cr^{III}. The unrestricted calculation on V^{II}-Cr^{III} employed the Gaussian 09 keyword "guess=alter" to change the initial guess wave function, where the following pairs of alpha-spin orbitals were switched: 96, 99; 97, 100; 98, 101. Out of curiosity, we also used the restricted formalism for closed electronic shells of the singlet spin V^{II}-Cr^{III} monomeric unit, since the total spin in this system cancel and leaves a singlet state. Of course, magnetic measurements[27] indicate that the spins are mainly localised on either Cr or V in an antiferromagnetic fashion and so the restricted approach, where all electrons are paired up in molecular orbitals, is probably not realistic. We use the conventional nomenclature in quantum chemistry and label the spin up/down projections as alpha and beta. We would like to point out that in the simplified binuclear cluster, the d_{xy} orbital, which lies in the plane perpendicular to the internuclear axis, will have a different energy to the two d orbitals that lie on the axis (d_{xz} and d_{yz}). In the 3D extended network this artefact would not be observed.

3. Results and discussion

One of the most striking results of all the calculations were the relatively few transitions observed and that these were quite “clean” one-electron transitions in specific molecular orbitals (MOs). The results for $V^{II/III}$-Cr^{III}, the stretched geometries of $V^{II/III}$-Cr^{III}, and Cr^{II}-Cr^{III} PBAs are presented below separately and in Tables 1 to 4.

3.1 $V^{II/III}$-Cr^{III} PBA

Unrestricted V^{II}-Cr^{III}. In the unrestricted calculation on the V^{II}-Cr^{III} binuclear unit, the Cr valence electrons are in the alpha channel with energies of 9.7 eV in MOs 93a and 94a corresponding to d_{xz} and d_{yz} MOs. Both these MOs are partially delocalised over the CN bridging ligand, as expected. MO 91a, corresponding to the d_{xy} orbital, has one electron with an energy of 9.6 eV but is not delocalised over the bridging ligand (because it lies in the xy plane). The slightly lower energy of the d_{xy} orbital is an artefact due to the binuclear model, as discussed in the methods section. There are ligand orbitals (MOs 95a−98a) at 9.9 – 10.2 eV, close in energy to the Cr MOs, in agreement with density-of-state calculations on the extended V-Cr PBA[28]. The HOMO is in the beta channel and corresponds to V d_{xz} and d_{yz} orbitals (MOs 97b and 98b), which occur at 13.5 eV. The d_{xy} MO has an energy of 13.4 eV (MO 96b). In the beta channel there are also ligand orbitals at 10.2 eV (lower in energy than the d-orbitals). These coincide with the ligand orbitals in the alpha channel. The energy difference between the d orbitals on Cr and V is 3.8 eV, which is also in reasonable agreement with the aforementioned density-of-state calculations on the extended V-Cr PBA [28] and recent ultraviolet photoelectron spectra on thin films (*to be published*). Furthermore, the calculations correctly predict opposite spin polarisations on the Cr and V ions. This spin polarisation arises due to the superexchange interaction, which in turn comes from the energy balance between the energy gain of aligning the spins in a ferromagnetic (FM) interaction (and thus reducing electron-electron repulsion) vs. delocalising and thereby lowering of the kinetic energy of the MO. By forming a delocalised MO, two electrons will be placed in the same MO and therefore align their spins antiferromagnetically (AFM). Because

of the bridging ligand, the FM interaction is weak and the kinetic term usually leads to the AFM ordering typically associated with the superexchange interaction.

In the calculated optical spectrum of V^{II}-Cr^{III} using the unrestricted formalism, MMCT and various ligand-to-metal charge-transfer (LMCT) and metal-to-ligand charge-transfer (MLCT) transitions were observed. Table 1 shows the predicted electronic transitions, in the wavelength range 400 to 800 nm, of the model binuclear unit with a V-Cr distance of 5.33 Å. In the visible/near-IR region of the spectrum there is only one transition, which is a MMCT from Cr to V at 743 nm. This transition involves the CT of a spin-down electron from V to Cr, involving transitions from MOs 97b to 100b and from 98b to 99b. These are the transitions between d_{xz} and d_{yz} MOs. The oscillator strength for these transitions is f = 0.16. There are LMCT transitions at around 258 nm but with small oscillator strengths from 0.0001 to 0.0030. We also observe an MLCT at 287 nm but with negligible oscillator strength (f = 0.0001). We also observe transitions at 294 nm corresponding to V to Cr *n*s Rydberg states. Again, these transitions have small oscillator strengths (f = 0.0001).

Restricted V^{II}-Cr^{III}. We also carried out restricted calculations on the V^{II}-Cr^{III} since there is an even number of electrons and the total spin of the system is zero due to the AFM nature of the superexchange interaction. The restricted formalism forces the electrons to pair up AFM in the MOs because of the Pauli exclusion principle. Since the optical properties might not necessarily be affected by the spin configuration at high temperatures[29], we were interested in investigating whether the restricted calculations would more accurately reproduce the transition energy of the MMCT. In the results of these calculations, the MOs were mixed between d-orbitals on both ions. In the restricted calculations, the HOMO is even more delocalised between the two metal centres, although the main electron density is still on the V, which has a fractional occupation of 0.52 from an orbital-by-orbital analysis (see Table 2), with the fraction 0.27 on the Cr ion. The energy of the HOMO was 13.3 eV and is thus close to the energy of the Cr ion in the unrestricted calculation. The total energy of the system was ca. 5.6 eV above the unrestricted calculation. This is certainly much

higher than the thermal energy available at room-temperature. Not surprisingly, there is a large difference in energy between two paramagnetic centres and the complete electron-paring in the restricted formalism. The TD-DFT results were otherwise in good agreement with the optical spectra, where the calculated value of the MMCT at 572 nm is close to the experimental value of 540 nm[17,18]. The transition itself is of mixed character, involving a transition from Cr d_{t2g} to V d_{t2g} and V d_{t2g} to Cr d_{t2g} orbitals. Further analysis of this transition suggests that this is dominated by a V d_{t2g} to Cr d_{t2g} transition. Table 2 displays characteristics of the molecular orbitals involved in the transitions for the V^{III}-Cr^{III} and V^{II}-Cr^{III} ground states of the model monomeric unit with a V-Cr distance of 5.33 Å. The orbital-by-orbital analysis gives the atomic contributions to the molecular orbitals. For V^{II}/Cr^{III} the transition to the ^1E state at 572 nm is a combination of two configurations (Tables 1 and 2): MO 97 to 99 and MO 98 to 100. Degenerate occupied MOs 97 and 98 have identical character and the orbital-by-orbital analysis indicates that they are localised more on the V^{II} ion. Analogously, the degenerate unoccupied MOs 99 and 100 have identical character and the orbital-by-orbital analysis indicates that they are localised more on the Cr^{III} ion. The calculations therefore indicate that this transition is dominated by the MMCT from V d_{t2g} to Cr d_{t2g}, similarly to the unrestricted calculations.

Unrestricted V^{III}-Cr^{III}. For the unrestricted calculations on V^{III}-Cr^{III}, the valence electron configuration was not as expected. Here two spin down electrons and one spin up electron were found on the Cr ions. The electron configuration was: $(d_{xz})^1$, $(d_{yz})^2$, and $(d_{xy})^0$. Clearly the calculations struggle for this open system. On the other hand, two spin up electrons were found on V, with the predicted oxidation state and spin configuration. The electron configuration on V was $(d_{xz})^1$, $(d_{xy})^1$. The electronic configuration on Cr might be an artefact of the bi-nuclear model since in the solid state there would be neighbouring MOs with matching symmetry.

In the TD-DFT results for V^{III}/Cr^{III}, two states accessible in the 400 to 800 nm region were observed; a Cr d_{t2g} to V d_{t2g} transition at 779 nm and a CN^- σ/π to Cr d_{t2g} transition at 401

nm. Both of the excited states of the V^{III}-Cr^{III} ground state are spin-contaminated triplets (the value of $\langle S^2 \rangle$ for a pure triplet is 2.00). Analysis of the two V^{III}/Cr^{III} transitions at 779 and 401 nm reveals that the excited states are both comprised of one configuration, as indicated by the Configuration Interaction (CI) Singles weights, where the CI weights are greater than |0.9| for both transitions (Table 1). These one-electron transitions arise from the MMCT from Cr d_{t2g} to V d_{t2g} (involving the HOMO and LUMO alpha spin MOs) and LMCT from ligand σ/π to Cr d_{t2g} (involving occupied beta-spin MO 92b to the LUMO beta spin MO).

Discussion of results for V^{II}-Cr^{III} and V^{III}-Cr^{III}. The calculated oscillator strengths for the MMCT transitions for the two vanadium oxidation states are quite different. From Table 1 it can be seen that the oscillator strength for the MMCT of V(II) is f = 0.16 and f = 0.80 for the unrestricted and restricted calculations, respectively. This is 4 and 20 times larger than the MMCT for V(III). It is interesting to notice that the molar extinction coefficients for V^{II}-Cr^{III} and V^{III}-Cr^{III} have both been measured by Garde *et al*. [17] in suspension of V-Cr PBA particles and their observations are in agreement with the calculations presented here. In fact, Garde *et al*. report that "*the molar absorption coefficients ε of the V(II)/chromicyanide solution are much higher (by a factor 15) than that of the V(III)/chromicyanide solution*". This ratio is in very good agreement with our findings. The larger oscillator strength is most likely due to the much larger delocalisation of the V^{II}-Cr^{III} system compared to the V^{III}-Cr^{III}. In particularly this is true for the excited state (see figure in Table 2). The restricted formalism, with its large delocalisation, naturally gives much larger oscillator strengths. The larger delocalisation is observed for both the restricted and unrestricted formalisms and can in turn be described by the relative energies of the V ions and the ligand orbitals[25]. The lower energy of the Cr(III) ions means that this ion interacts with occupied ligand orbitals and forms a molecular orbital with these (σ-donation). Therefore, the Cr ions accept electron density from the ligands. The V(II) ions' orbitals are much further up in energy and so interact with the empty ligand orbitals. They therefore donate density into the ligands (π-backbonding). One can see how this leads to delocalisation, whereas for the V(III) case, which is closer to the occupied ligand

orbitals, there will be a competition for electron density from the ligand between the Cr(III) and V(III) ions. The increase in oxidation state with the decrease of π-backbonding was recently observed directly in resonant inelastic X-ray scattering (RIXS) experiments[30]. The destabilisation of the CN^- ligand upon π-backbonding is generally manifested in the decrease in IR frequency of the asymmetric cyanide stretch mode [31]. This trend was also observed in the $V^{II/III}$-Cr^{III} PBA[27]. There is therefore a balance where V(II) donates electrons to the ligands and Cr(III) accepts them. Our calculations capture this degree of delocalisation, which has also been described for the magnetic properties. We have therefore shown that the photophysics can also be described based on an analysis of the delocalisation from the TD-DFT calculations.

3.2 Stretched V-Cr PBA

In order to computationally investigate the dependence of the MMCT transition on the bond length, we carried out calculations using an artificially longer internuclear distance. For this 'stretched' geometry (V-Cr distance of 5.75 Å), in the restricted calculation for the V^{II}/Cr^{III} oxidation state, the Cr d_{t2g} to V d_{t2g} and V d_{t2g} to Cr d_{t2g} transition is red-shifted from 572 nm to 1060 nm. The oscillator strength has been reduced from 0.783 to 0.219 for the stretched geometry. Tables 3 and 4 display, respectively, the transition energies and the molecular orbital characteristics. The stretched geometry, with its significantly lower degree of delocalisation, does show that the energy of the MMCT is significantly decreased, however, the direction of the CT is reversed (refer to the transition dipole moments for the ^1E states in Tables 1 and 3). For the stretched geometry, this transition is dominated by CT from Cr to V (Tables 3 and 4). For the V^{III}-Cr^{III} the stretched geometry produced no MMCT (or any other transition) in the visible region of the spectrum. The first transition with f>0.01 occurred at 278 nm (f = 0.02) and was a LMCT to V.

3.3 Cr^{II}-Cr^{III} PBA

Upon exchanging V^{II} to Cr^{II} in the PBA model binuclear unit, i.e. Cr^{II}-Cr^{III} PBA with a Cr-Cr distance of 5.33 Å, TD-DFT predicts two MMCT transitions at 284 and 266 nm (Table 1). The two Cr ions are labelled as Cr14, which is surrounded by the nitrogen end of the cyano ligand, and Cr3, which is bound to the carbon end of the ligand. The oxidation states of the two Cr ions, i.e. which is Cr^{II} and which is Cr^{III}, is difficult to assign. An orbital-by-orbital analysis yields the following: Cr3 has two alpha electrons in the d_{yz} and d_{xy} orbitals (MOs 97a and 98a) and one beta electron in the d_{xz} orbital (MO 98b). Cr14 has one alpha electron in the d_{xy} orbital (MO 96a) and two beta electrons in the d_{yz} and d_{xz} orbitals (MOs 96b and 97b). The HOMO (MO 99a) is in the alpha channel with an energy of 13.8 eV. It is delocalised in d_{xz}-type atomic orbitals on both Cr ions as Cr14 (0.41) and Cr3 (0.34), where atomic contributions are in parentheses. The larger atomic contribution on Cr14 is therefore consistent with the general assumption that Cr in the N-pocket is typically Cr^{II}. The predicted oscillator strength for the MMCT transition at 284 nm is two orders of magnitude greater than for the MMCT transition at 266 nm (Table 1). This may be due to the fact that the virtual orbital (MO 101b) for the latter, weaker transition is less localised than the virtual orbital (MO 101a) involved in the former, more intense transition (Table 2). However, the oscillator strength of the stronger transition is still rather weak and is comparable to the MMCT in V^{III}/Cr^{III} PBA. Furthermore, the similarity extends further because, as predicted for the V^{III}/Cr^{III} PBA, the two MMCT transitions for Cr^{II}/Cr^{III} are dominated by one configuration in forming the excited states. However, the degree of delocalisation is larger for the Cr^{II}-Cr^{III} PBA than for the V^{III}-Cr^{III} PBA. This not surprising since the magnetic transition temperature for Cr-Cr is typically rather high, first reported to be $T_c \approx 240$ K[21]. The rather large delocalisation of the HOMO is in agreement with the relatively high T_c, which has been observed previously in several computational studies. However, since the MMCT is from the more localised HOMO-2 the corresponding oscillator strength is weaker than that expected from the delocalisation of the HOMO. This shows that the oscillator strength of the MMCT is not necessarily directly

related to the T_c and our TD-DFT calculations output a reasonable MMCT oscillator strength. We note that the predicted spectral positions of the MMCT transitions are in agreement with the assignment made by Coronado *et al.* [19].

In addition to the MMCT transitions, we also observe LMCT transitions (with oscillator strengths) at 304 (0.0004), 294 (0.0064), 275 (0.0025), 272 (0.0026) and 260 nm (0.0011 au), and MLCT transitions at 294 (0.0228), 272 (0.0175) and 266 nm (0.0087 au). Interestingly, we also observe Cr d_{t2g} to Cr s-type orbital Rydberg transitions in the UV region at 301 (0.0002) and 260 nm (0.003 au).

4. Conclusion

We have carried out TD-DFT calculations on a series of binuclear hexacyanochromate PBAs. The results show that the TD-DFT calculations can correctly place the relative energies of MMCT transitions for $V^{II/III}$-Cr^{III} PBAs in agreement with experiments (calc. values for V^{II}-Cr^{III} at 572 and 743 nm for the restricted and unrestricted formalisms, respectively; and 779 nm for V^{III}-Cr^{III}). The calculations also give the relative transition strength in agreement with experiments, and we found f = 0.16 for V(II) and f = 0.038 for V(III). The calculations also predicted that the MMCT of $Cr^{II}Cr^{III}$ occurs in the UV at 284 nm. The corresponding oscillator strength for this transition was weak due to the localised nature of "optical" orbitals. However, the HOMO had a larger degree of delocalistion. We find that the unrestricted calculations work best if there are equal numbers of electrons on either sites, as for V^{II}-Cr^{III}.

Our findings show that TD-DFT calculations are useful for understanding and predicting optical properties of Prussian blue analogues. With a huge range of potential applications of the PBAs in multifunctional materials, including magnetic, piezoelectric, batteries, and electrochromic devices, a computational approach to screen the optical properties is highly desirable.

Acknowledgements

JOJ acknowledges financial support from the Royal Society of Edinburgh. JOJ is a Royal Society of Edinburgh/BP Trust Research Fellow. The computational work has made use of the resources provided by the EaStCHEM Research Computing Facility at the University of Edinburgh.

References

[1] M. Verdaguer, G.S. Girolami, Magnetic Prussian Blue Analogs, in: J.S. Miller, M. Drillon (Eds.), Magn. Mol. to Mater., Wiley-VCH Verlag GmbH & Co. KGaA, Weinheim, Germany, 2005: pp. 283–346. doi:10.1002/9783527620548.ch9d.

[2] O. Sato, T. Iyoda, A. Fujishima, K. Hashimoto, Photoinduced Magnetization of a Cobalt-Iron Cyanide, Science. 272 (1996) 704–705. http://www.ncbi.nlm.nih.gov/pubmed/8662564.

[3] S. Ohkoshi, H. Tokoro, Photomagnetism in Cyano-Bridged Bimetal Assemblies, Acc. Chem. Res. 45 (2012) 1749–1758. doi:10.1021/ar300068k.

[4] P.R. Somani, S. Radhakrishnan, Electrochromic materials and devices: present and future, Mater. Chem. Phys. 77 (2003) 117–133. doi:10.1016/S0254-0584(01)00575-2.

[5] P.M.S. Monk, R.J. Mortimer, D.R. Rosseinsky, Electrochromism by intervalence charge-transfer coloration: metal hexacyanometallates, in: Electrochromism and Electrochromic Devices, Cambridge University Press, Cambridge, 2007: pp. 282–302.

[6] M. Verdaguer, M. Glavez, R. Garde, C. Desplanches, Electrons at Work in Prussian Blue Analogues, Electrochem. Soc. Interface. 11 (2002) 28.

[7] M. Verdaguer, A. Bleuzen, C. Train, R. Garde, F. Fabrizi de Biani, C. Desplanches, Room-temperature molecule-based magnets, Philos. Trans. R. Soc. A Math. Phys. Eng. Sci. 357 (1999) 2959–2976. doi:10.1098/rsta.1999.0476.

[8] L. Hedley, N. Robertson, J.O. Johansson, Electrochromic Thin Films of the V-Cr Prussian Blue Analogue Molecular Magnet, Electrochim. Acta. 236 (2017) 97–103. doi:10.1016/j.electacta.2017.03.166.

[9] S. DeBeer George, T. Petrenko, F. Neese, Prediction of Iron K-Edge Absorption Spectra Using Time-Dependent Density Functional Theory †, J. Phys. Chem. A. 112 (2008) 12936–12943. doi:10.1021/jp803174m.

[10] F. De Angelis, A. Tilocca, A. Selloni, Time-Dependent DFT Study of [Fe(CN) 6] 4- Sensitization of TiO 2 Nanoparticles, J. Am. Chem. Soc. 126 (2004) 15024–15025. doi:10.1021/ja045152z.

[11] Y. Kitagawa, M. Asaoka, K. Miyagi, T. Matsui, M. Nihei, H. Oshio, M. Okumura, M. Nakano, DFT and TD-DFT studies of electronic structures and one-electron excitation states of a cyanide-bridged molecular square complex, Inorg. Chem. Front. 2 (2015) 771–779. doi:10.1039/C5QI00091B.

[12] M.B. Robin, P. Day, Mixed Valence Chemistry-A Survey and Classification, Adv. Inorg. Chem. Radiochem. 10 (1968) 247–422. doi:10.1016/S0065-2792(08)60179-X.

[13] B. Mayoh, P. Day, Charge transfer in mixed valence solids. Part VII. Perturbation calculations of valence delocalization in iron(II,III) cyanides and silicates, J. Chem. Soc. Dalt. Trans. (1974) 846. doi:10.1039/dt9740000846.

[14] M.B. Robin, The color and electronic configurations of Prussian blue, Inorg. Chem. 1 (1962) 337–342. http://pubs.acs.org/doi/abs/10.1021/ic50002a028 (accessed March 27, 2014).

[15] S. Ohkoshi, A. Fujishima, K. Hashimoto, Transparent and Colored Magnetic Thin Films: (Fe II x Cr II 1- x) 1.5 [Cr III (CN) 6], J. Am. Chem. Soc. 120 (1998) 5349–5350. doi:10.1021/ja980732f.

[16] M. Mizuno, S. Ohkoshi, K. Hashimoto, Electrochemical Synthesis of High- Tc, Colored, Magnetic Thin Films Composed of Vanadium (II/III)–Chromium (II) Hexacyanochromate (III), Adv. Mater. 8904 (2000) 1955–1958. doi:10.1002/1521.

[17] R. Garde, F. Villain, M. Verdaguer, Molecule-Based Room-Temperature Magnets: Catalytic Role of V(III) in the Synthesis of Vanadium−Chromium Prussian Blue Analogues, J. Am. Chem. Soc. 124 (2002) 10531–10538. doi:10.1021/ja020528z.

[18] S. Ohkoshi, M. Mizuno, G. Hung, K. Hashimoto, Magnetooptical Effects of Room Temperature Molecular-Based Magnetic Films Composed of Vanadium Hexacyanochromates, J. Phys. Chem. B. 104 (2000) 9365–9367. doi:10.1021/jp002002b.

[19] E. Coronado, M. Makarewicz, J.P. Prieto-Ruiz, H. Prima-García, F.M. Romero, Magneto-optical properties of electrodeposited thin films of the molecule-based magnet Cr(5.5) (CN)(12) ·11.5H(2) O., Adv. Mater. 23 (2011) 4323–6. doi:10.1002/adma.201101513.

[20] J.O. Johansson, J.-W. Kim, E. Allwright, D.M. Rogers, N. Robertson, J.-Y. Bigot, Directly probing spin dynamics in a molecular magnet with femtosecond time-resolution, Chem. Sci. 7 (2016) 7061–7067. doi:10.1039/C6SC01105E.

[21] T. Mallah, S. Thiebaut, M. Verdaguer, P. Veillet, High-TC molecular-based magnets: ferrimagnetic mixed-valence chromium (III)-chromium (II) cyanides with TC at 240 and 190 Kelvin, Science (80-.). 262 (1993) 1554–1557. http://www.sciencemag.org/content/262/5139/1554.short (accessed October 31, 2013).

[22] M. Nishino, S. Takcda, W. Mori, A. Nakamura, K. Yamaguchi, Theoretical studies of organometallic conjugated systems: Prussian blue analogs, Synth. Met. 85 (1997) 1763–1764. doi:10.1016/S0379-6779(97)80426-2.

[23] M. Nishino, S. Kubo, Y. Yoshioka, A. Nakamura, K. Yamaguchi, Theoretical Studies on Magnetic Interactions in Prussian Blue Analogs and Active Controls of Spin States by External Fields, Mol. Cryst. Liq. Cryst. Sci. Technol. Sect. A. Mol. Cryst. Liq. Cryst. 305 (1997) 109–128. doi:10.1080/10587259708045050.

[24] M. Nishino, Y. Yoshioka, K. Yamaguchi, Effective exchange interactions and magnetic phase transition temperatures in Prussian blue analogs: a study by density functional theory, Chem. Phys. Lett. 297 (1998) 51–59. doi:10.1016/S0009-2614(98)01081-1.

[25] E. Ruiz, A. Rodríguez-Fortea, S. Alvarez, M. Verdaguer, Is It Possible To Get High T C Magnets with Prussian Blue Analogues? A Theoretical Prospect, Chem. - A Eur. J. 11 (2005) 2135–2144. doi:10.1002/chem.200400821.

[26] W.E. Buschmann, S.C. Paulson, C.M. Wynn, M.A. Girtu, A.J. Epstein, H.S. White, J.S. Miller, Reversed (Negative) Magnetization for Electrochemically Deposited High-

T c Thin Films of Chromium Hexacyanide Magnets, Chem. Mater. 10 (1998) 1386–1395. doi:10.1021/cm970773v.

[27] S. Ferlay, T. Mallah, R. Ouahès, P. Veillet, M. Verdaguer, A room-temperature organometallic magnet based on Prussian blue, Nature. 378 (1995) 701–703. doi:10.1038/378701a0.

[28] D.S. Middlemiss, L.M. Lawton, C.C. Wilson, A solid-state hybrid density functional theory study of Prussian blue analogues and related chlorides at pressure, J. Phys. Condens. Matter. 20 (2008) 335231. doi:10.1088/0953-8984/20/33/335231.

[29] P.A. Cox, Electron transfer between exchange-coupled ions in a mixed-valency compound, Chem. Phys. Lett. 69 (1980) 340–343. doi:10.1016/0009-2614(80)85076-7.

[30] K. Kunnus, W. Zhang, M.G. Delcey, R. V. Pinjari, P.S. Miedema, S. Schreck, W. Quevedo, H. Schröder, A. Föhlisch, K.J. Gaffney, M. Lundberg, M. Odelius, P. Wernet, Viewing the Valence Electronic Structure of Ferric and Ferrous Hexacyanide in Solution from the Fe and Cyanide Perspectives, J. Phys. Chem. B. 120 (2016) 7182–7194. doi:10.1021/acs.jpcb.6b04751.

[31] L.H. Jones, Nature of Bonding in Metal Cyanide Complexes as Related to Intensity and Frequency of Infrared Absorption Spectra, Inorg. Chem. 2 (1963) 777–780. doi:10.1021/ic50008a027.

Figures and tables

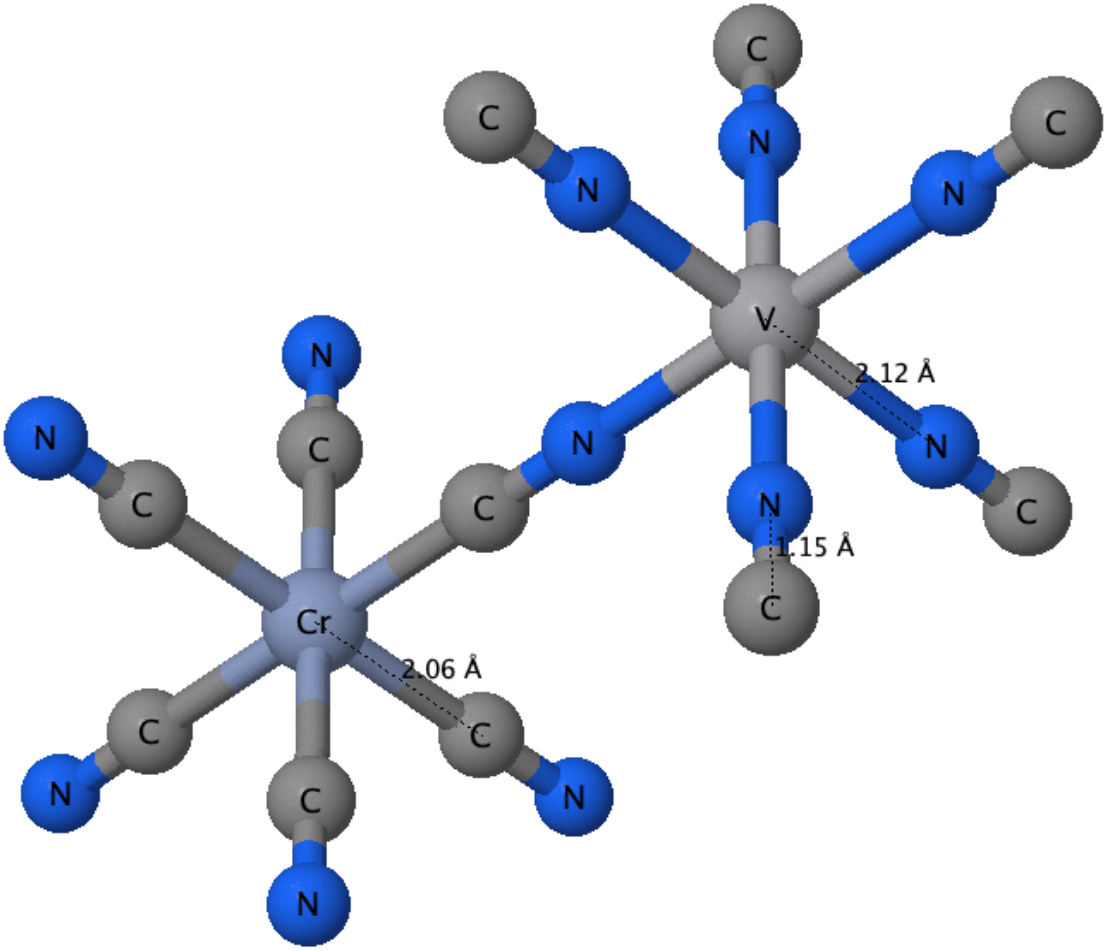

Figure 1. The model binuclear unit of V-Cr PBA used to perform the calculations. Bond lengths in Ångstroms.

State symmetry	E (eV)	E (nm)	*f* (au)	$\langle S^2 \rangle$	TDM (au)	Molecular orbitals (with CI coefficient)[a,b]	Transition
V^{II}-Cr^{III} unrestricted calculation (E = −3007.210893 hartrees, Q = −6 au, *S* = 1.3023, $\langle S^2 \rangle$ = 2.9983)							
^{3}E	1.67	743 (550)	0.1597	2.260	0.0 0.0 −1.9758	97b to 100b (0.70651); 98b to 99b (0.70651)	V d_{t2g} to Cr d_{t2g}
V^{II}-Cr^{III} restricted calculation (E = −3007.004408 hartrees, Q = −6 au, *S* = 0.0, $\langle S^2 \rangle$ = 0.0)							
^{1}E	2.17	572 (550)	0.7830	0.0	0.0 0.0 −3.8390	97 to 99 (0.66498); 98 to 100 (0.66498)	V/Cr d_{t2g} to Cr/V d_{t2g}
V^{III}-Cr^{III} (E = −3007.578133 hartrees, Q = −5 au, *S* = 0.9218, $\langle S^2 \rangle$ = 1.7714)							
^{3}A	1.59	779 (650)	0.0378	2.864	0.0 0.0 0.9704	98a to 99a (0.99464)	Cr d_{t2g} to V d_{t2g}
^{3}A	3.09	401	0.0033	3.241	−0.2091 0.0 0.0	92b to 98b (0.93215)	CN^- σ/π to Cr d_{t2g}
Cr^{II}-Cr^{III} (E = −3107.558507 hartrees, Q = −6 au, *S* = 1.2421, $\langle S^2 \rangle$ = 2.7851)							
^{3}A	4.36	284 (510, 610, 380)	0.0193	2.020	0.0 0.0 −0.4246	97a to 101a (0.97703)	Cr3 d_{t2g} to Cr14 d_{t2g}
^{3}A	4.65	266	0.0003	2.534	0.0 0.0544	97b to 101b (0.97873)	Cr14 d_{t2g} to Cr3 d_{t2g}

					0.0		

[a] For CI coefficients with weights greater than |0.5|. [b] a denotes alpha spin and b beta spin. [C] The unrestricted ground state has S = 1.30 and $\langle S^2 \rangle$ = 3.00 indicating that it is spin contaminated to a triplet state.

Table 1. TD-DFT predicted UV/Vis electronic transitions for the V^{III}-Cr^{III} and V^{II}-Cr^{III} oxidation states of the V-Cr PBA monomeric unit with a V-Cr distance of 5.33 Å. V^{III}-Cr^{III} is identified as $^2B_1$ and V^{II}-Cr^{III} as $^1A_1$. Results for the Cr^{II}-Cr^{III} $^2B_1$ state of Cr-Cr PBA are also shown. Excited states of undetermined spatial symmetry are labelled as A (i.e. C_1 symmetry). Where available, experimental values from the literature are also shown in parenthesis. The value for V^{II}/Cr^{III} and V^{III}/Cr^{III} are from ref. [17,18] and for Cr-Cr from ref. [15,19].

Molecular orbital[a]	**Energy (Hartrees)**	**Orbital-by-orbital analysis[b]**	**Contour plot of molecular orbital[c]**
V^{II}-Cr^{III} unrestricted calculation			
97b (HOMO−1)	0.495	V14 d_{t2g} (0.81)	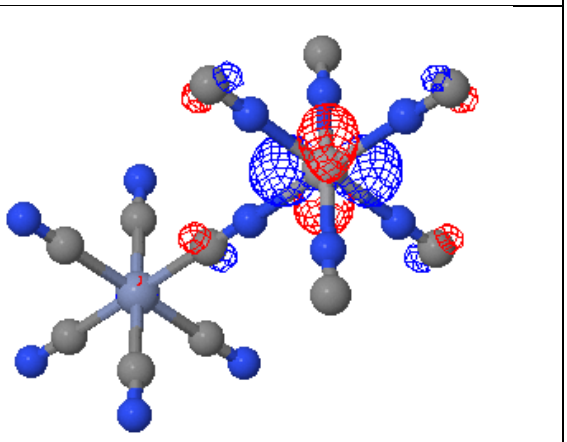
98b (HOMO)	0.495	V14 d_{t2g} (0.81)	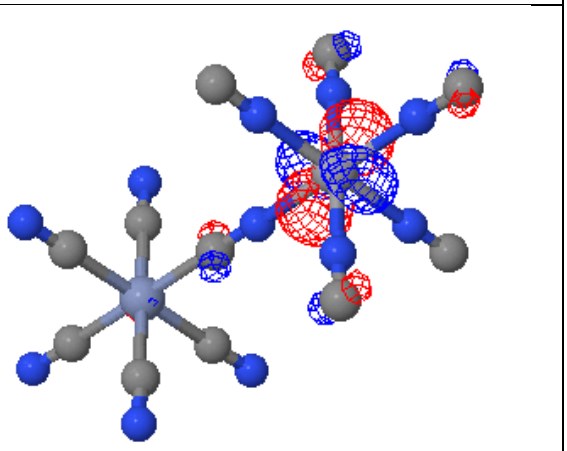
99b (LUMO)	0.574	Cr3 d_{t2g} (0.50)	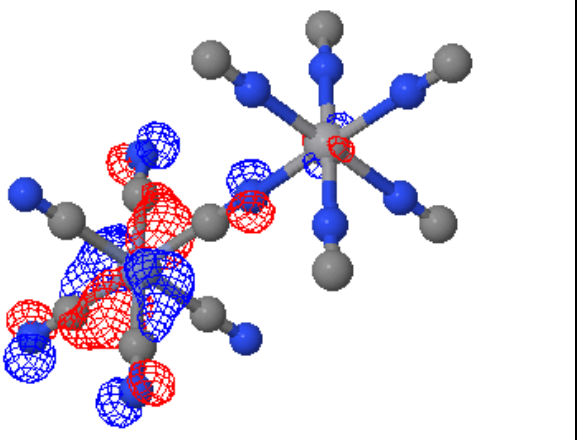

100b (LUMO+1)	0.574	Cr3 d_{t2g} (0.50)	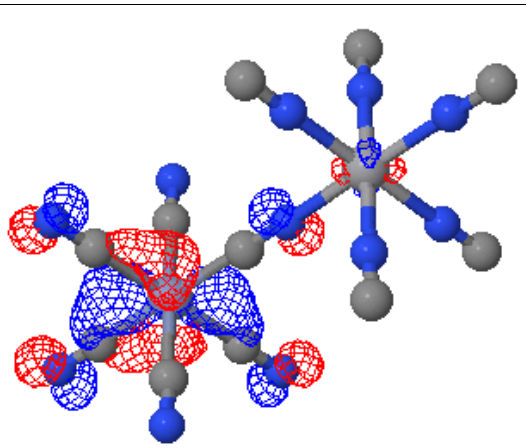
V^{II}-Cr^{III} restricted calculation			
97 (HOMO−1)	0.490	V14 d_{t2g} (0.52), Cr3 d_{t2g} (0.27)	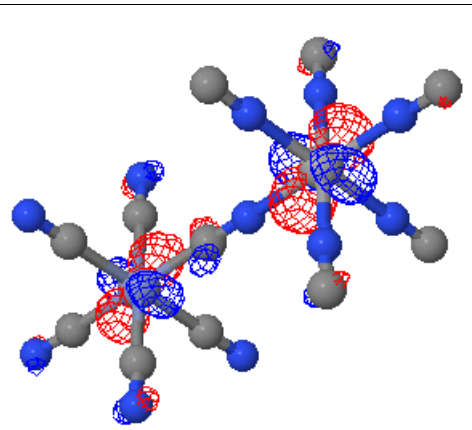
98 (HOMO)	0.490	V14 d_{t2g} (0.52), Cr3 d_{t2g} (0.27)	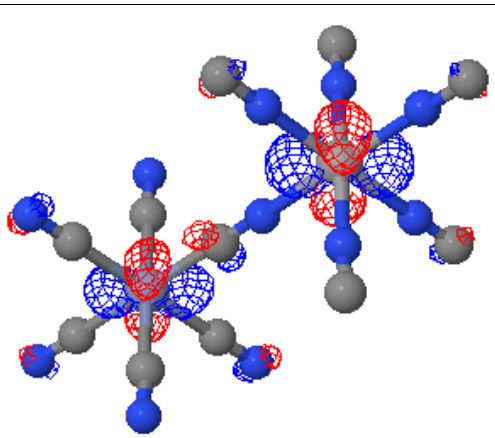

99 (LUMO)	0.532	Cr3 d_{t2g} (0.48), V14 d_{t2g} (0.31)	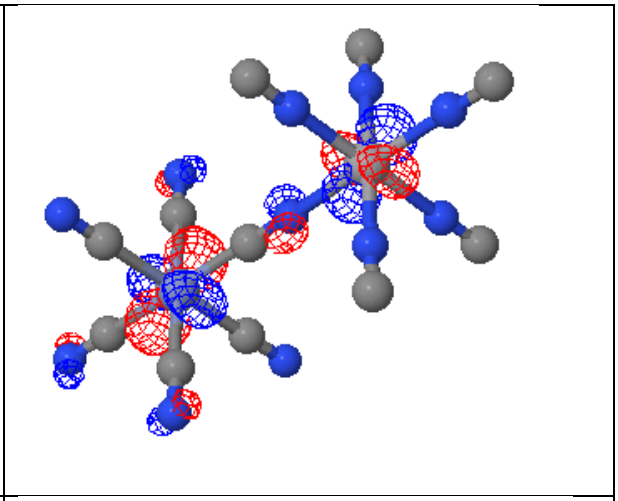
100 (LUMO+1)	0.532	Cr3 d_{t2g} (0.48), V14 d_{t2g} (0.31)	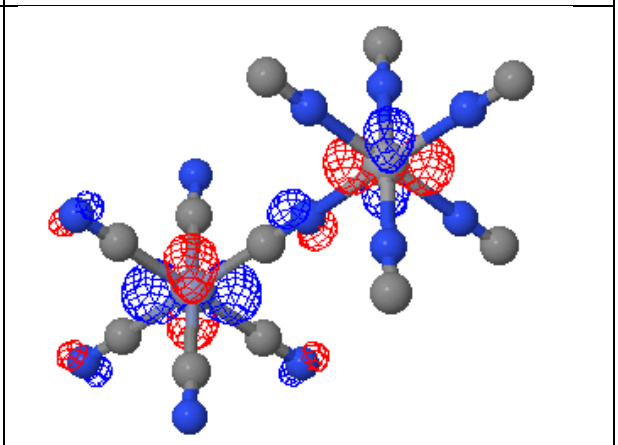
V^{III}-Cr^{III}			
92b (beta HOMO−6)	0.222	C8 p (0.12), C4 p (0.12)	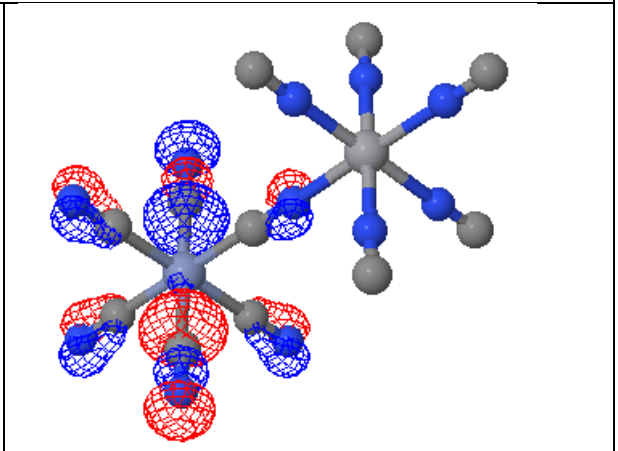

98a (alpha HOMO)	0.319	Cr3 d_{t2g} (0.78)	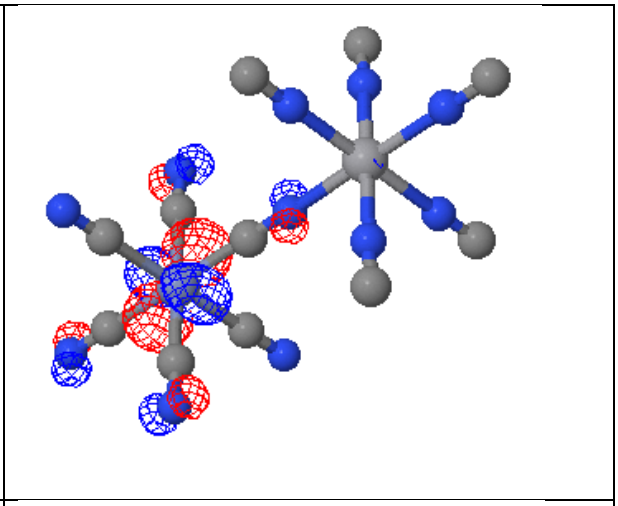
98b (beta LUMO)	0.396	Cr3 d_{t2g} (0.77)	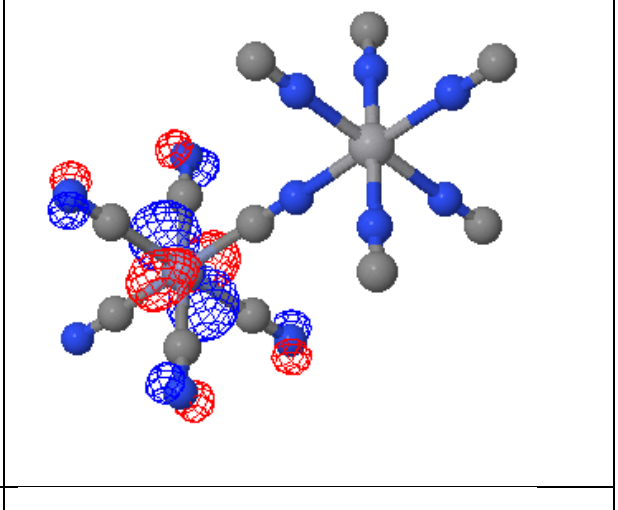
99a (alpha LUMO)	0.405	V14 d_{t2g} (0.83)	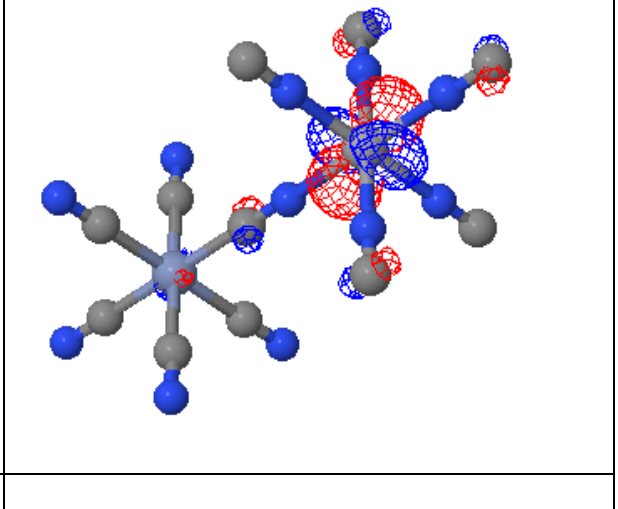
Cr^{II}-Cr^{III}			

97a (alpha HOMO−2)	0.411	Cr3 d_{t2g} (0.79)	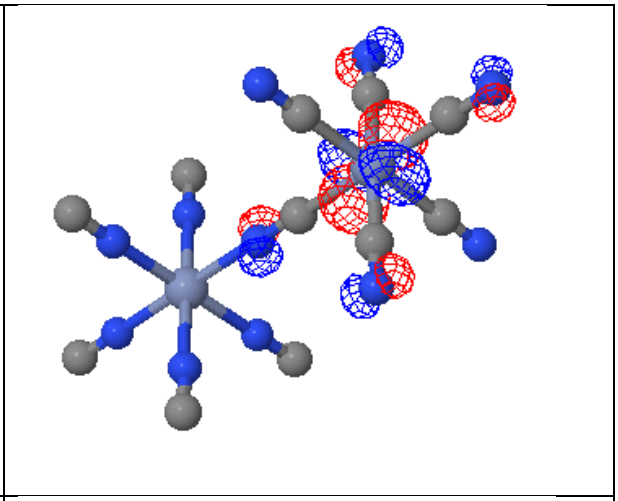
97b (beta HOMO−1)	0.408	Cr14 d_{t2g} (0.82)	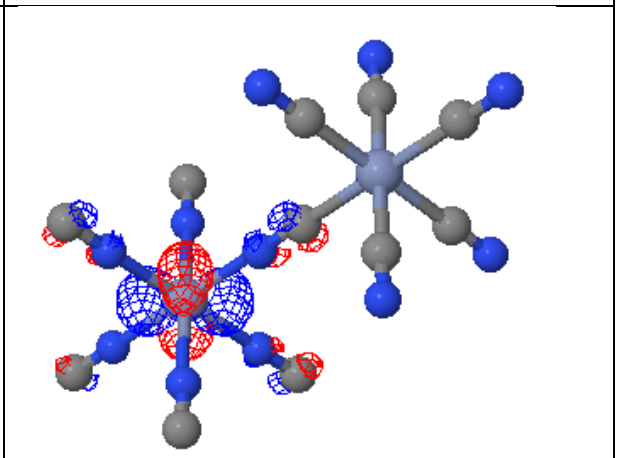
101a (alpha LUMO+1)	0.599	Cr14 d_{t2g} (0.72)	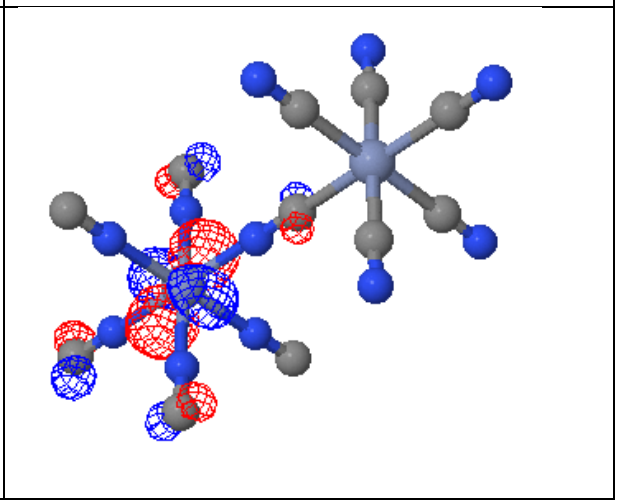

101b (beta LUMO+2)	0.605	Cr3 d_{t2g} (0.53)	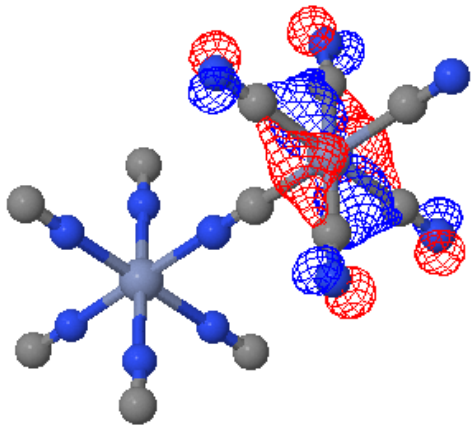

[a] a denotes alpha spin and b beta spin. [b] atom, orbital type and fractional atomic contribution in parentheses. [c] the Cr ion is on the left of the plot. For V^{III}-Cr^{III} the alpha HOMO is MO 98a and the beta HOMO is MO 97b. For V^{II}-Cr^{III} the HOMO is MO 98. For Cr^{II}-Cr^{III} the alpha HOMO is MO 99a and the beta HOMO is MO 98b. The d-type atomic orbitals were assigned as d_{t2g} by visual inspection.

Table 2. Characteristics of the molecular orbitals involved in the transitions in the model monomeric units of the V-Cr and Cr-Cr PBAs with inter ion distances of 5.33 Å.

State symmetry	E (eV)	E (nm)	*f* (au)	<S^2>	TDM (au)	Molecular orbitals (with CI coefficient)[a,b]	Transition
V^{III}-Cr^{III} (E = −3007.623971 hartrees, Q = −5 au, *S* = 1.2381, ⟨S^2⟩ = 2.7711)							
^{4}A	4.46	278	0.0199	3.989	0.4261 0.0 0.0	71a to 99a (0.88826)	CN^- pi to V d_{t2g}
V^{II}-Cr^{III} restricted calculation (E = −3007.033566 hartrees, Q = −6 au, *S* = 0.0, ⟨S^2⟩ = 0.0)							
^{1}E	1.17	1060	0.2189	0.0	0.0 0.0 2.7644	97 to 100 (0.57007); 98 to 99 (0.57007)	Cr d_{t2g} to V d_{t2g}

[a] For CI coefficients with weights greater than 0.5. [b] a denotes alpha spin and b beta spin.

Table 3. TD-DFT predicted UV/Vis electronic transitions for the V^{III}-Cr^{III} and V^{II}-Cr^{III} oxidation states of the V-Cr PBA monomeric unit with a 'stretched' V-Cr distance of 5.75 Å. V^{III}-Cr^{III} is identified as $^2B_1$ and V^{II}-Cr^{III} as $^1A_1$. Excited states of undetermined spatial symmetry are labelled as A (i.e. C_1 symmetry).

Molecular orbital[a]	**Energy (Hartrees)**	**Orbital-by-orbital analysis[b]**	**Contour plot of molecular orbital[c]**
V^{III}-Cr^{III}			
71a (alpha HOMO−27)	0.172	N21 p (0.18), N17 p (0.18)	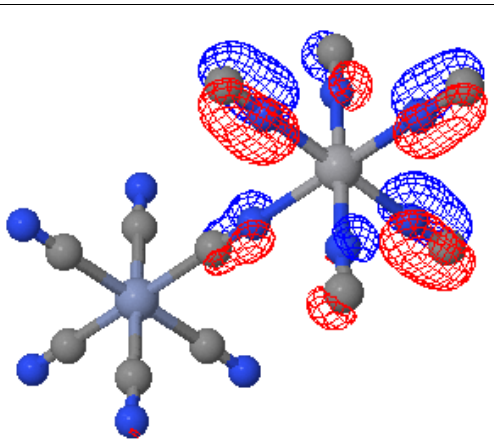
99a (alpha LUMO)	0.387	V14 d_{t2g} (0.85)	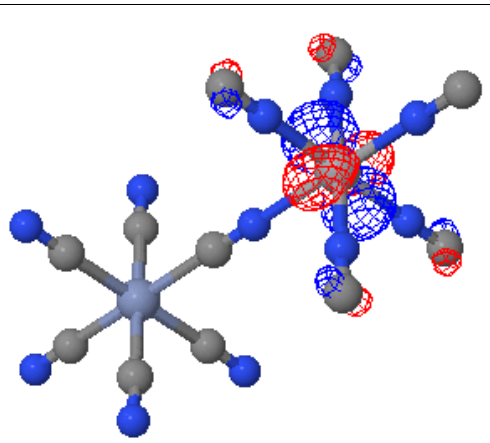
V^{II}-Cr^{III}			

97 (HOMO−1)	0.484	Cr3 d_{t2g} (0.74)	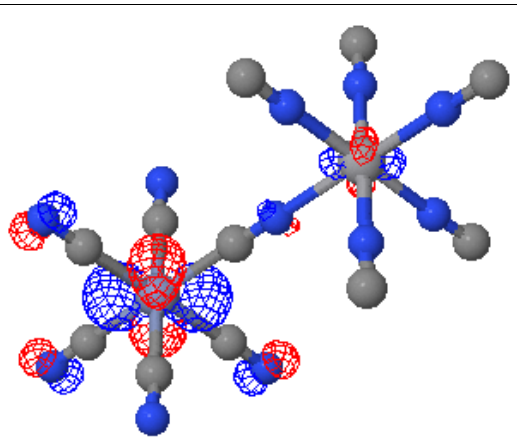
98 (HOMO)	0.484	Cr3 d_{t2g} (0.74)	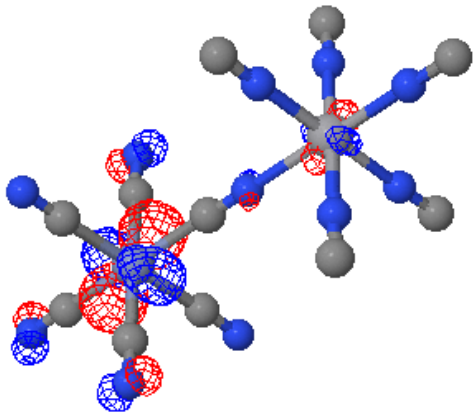
99 (LUMO)	0.521	V14 d_{t2g} (0.78)	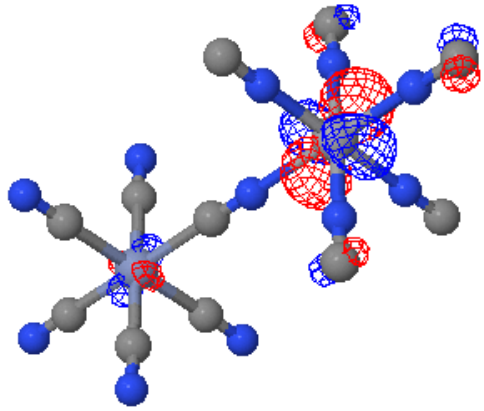

100 (LUMO+1)	0.521	V14 d_{t2g} (0.78)	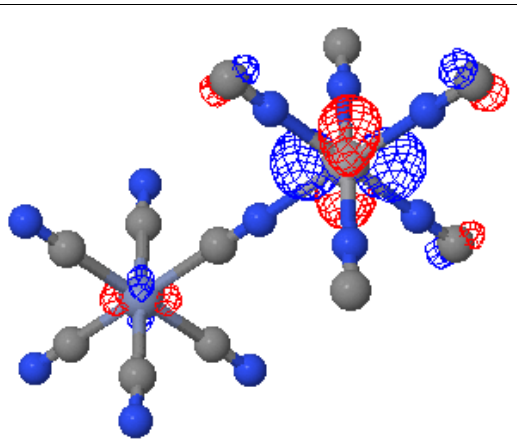

[a] a denotes alpha spin and b beta spin. [b] atom, orbital type and fractional atomic contribution in parentheses. [c] the Cr ion is on the left of the plot. For V^{III}-Cr^{III} the alpha HOMO is MO 98a and the beta HOMO is MO 97b. For V^{II}-Cr^{III} the HOMO is MO 98. The d-type atomic orbitals were assigned as d_{t2g} by visual inspection.

Table 4. Characteristics of the molecular orbitals involved in the transitions in the model monomeric unit of the V-Cr PBA with an inter ion distance of 5.75 Å.